ACS APPLIED MATERIALS & INTERFACES

Research Article

www.acsami.org

Oxygen-Free Atomic Layer Deposition of Indium Sulfide

Robert F. McCarthy,[†] Matthew S. Weimer,[§,†] Jonathan D. Emery,[†] Adam S. Hock,[‡,§] and Alex B. F. Martinson*[,†]

[†]Materials Science Division and [‡]Chemical Sciences and Engineering Division, Argonne National Laboratory, 9700 South Cass Avenue, Argonne, Illinois 60439, United States

[§]Department of Biological and Chemical Sciences, Illinois Institute of Technology, 3101 South Dearborn Street, Chicago, Illinois 60616, United States

Supporting Information

ABSTRACT: Atomic layer deposition (ALD) of indium sulfide (In_2S_3) films was achieved using a newly synthesized indium precursor and hydrogen sulfide. We obtain dense and adherent thin films free from halide and oxygen impurities. Self-limiting half-reactions are demonstrated at temperatures up to 225 °C, where oriented crystalline thin films are obtained without further annealing. Low-temperature growth of 0.89 Å/cycle is observed at 150 °C, while higher growth temperatures gradually reduce the per-cycle growth rate. Rutherford backscattering spectroscopy (RBS) together with depth-profiling Auger electron spectroscopy (AES) reveal a S/In ratio of 1.5 with no detectable carbon, nitrogen, halogen, or oxygen impurities. The resistivity of thin films prior to air exposure decreases with increasing deposition temperature, reaching <1 Ω·cm for films deposited at 225 °C. Hall measurements reveal n-type conductivity due to free electron concentrations up to 10^{18} cm^{-3} and mobilities of order 1 $cm^2/(V·s)$. The digital synthesis of In_2S_3 via ALD at temperatures up to 225 °C may allow high quality thin films to be leveraged in optoelectronic devices including photovoltaic absorbers, buffer layers, and intermediate band materials.

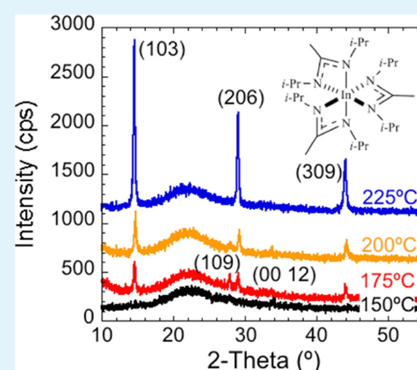

KEYWORDS: *Atomic layer deposition, indium sulfide, in situ measurements, surface reactions, indium(III) amidinate, photovoltaics*

INTRODUCTION

Indium sulfide has long attracted attention as one of just a few simple sulfides with good stability, moderate band gap, and high carrier mobility. In_2S_3 has shown potential, in particular, in the photovoltaic industry as a buffer layer in thin film devices,[1,2] with potential to replace toxic CdS layers. Indium(III) is also a principal component in some of the most efficient thin film chalcogenide PV alloys including $CuInS_2$ and Cu(In,Ga)-$(S,Se)_2$. In addition to these supporting roles, In_2S_3 may serve as a well-behaved and photoactive absorber layer. Substitutionally doped alloys of In_2S_3 have further been identified as impurity-band absorbers with nearly ideal energy level separation for solar energy applications.[3,4] A variety of deposition methods exist for In_2S_3 including chemical bath deposition,[5−7] physical vapor deposition,[7,8] ion layer gas reaction,[9,10] sputtering,[11] and atomic layer deposition (ALD).[12−14] ALD is one of the most promising routes to optoelectronic materials, as it enables digital control and conformal growth, sophisticated doping opportunities, as well as pinhole-free films of high density.[15,16]

The self-limiting surface chemistries that constitute a well-defined ALD process afford unique synthetic control over interfaces, stoichiometry, and crystalline phase.[17] Furthermore, many low-temperature ALD (<200 °C) processes have been identified that enable high quality materials growth in applications with limited thermal stability including flexible substrates[18,19] or multilayers prone to diffusion.[20,21] An important requirement for achieving electronic-quality materials through low-temperature ALD is the identification and synthesis of a metal precursor with clean surface chemistry that results in the material of interest and avoids deleterious impurities. Though several reports of the ALD of In_2S_3 have been published,[12,22] the processes leave something to be desired. Initial work with $InCl_3$ showed good growth rates of 1.4 Å/cycle and lead to polycrystalline films. However, a volatilization temperature of at least 300 °C is required for $InCl_3$, which necessitates the use of more complex tooling, including high temperature and chemically resistant valves. Composition analysis also revealed that optimized growth resulted in 3% Cl contamination, a value that is well beyond that acceptable for many applications.[12] In an attempt to bypass high temperature halide-based processes, which produce strongly acidic byproducts known to etch films and damage tools,[23−25] several reports have focused on indium(III) acetylacetonate $(In(acac)_3)$. This precursor allows for significantly lower growth temperatures and halide-free films when dosed alternately with H_2S.[14] However, a wide range of thin film properties result including an observed direct band gap of

Received: March 5, 2014
Accepted: July 15, 2014
Published: July 25, 2014

 © 2014 American Chemical Society dx.doi.org/10.1021/am501331w | *ACS Appl. Mater. Interfaces* 2014, 6, 12137−12145

~2.8 eV[26,27] consistent with significant oxygen incorporation.[28] The precursor is further limited by a modest thermal stability threshold reported to be 150 °C.[29] The resulting films exhibit nonideal S/In ratios (1.42)[13,22] and high carbon levels (3.7−5.1%),[13,22] while the process suffers from low precursor volatility[13,14] and modest self-limiting growth rates −0.35 Å/cycle with demonstrated self-limiting behavior, though up to 0.7 Å/cycle has been reported,[13] that all leave significant room for improvement.

Until now, there have been no reports of In_2S_3 thin films grown by ALD with an impurity level lower than 3%. In search of more facile surface chemistry certain to be free of halide and oxygen contamination, we screened several commercially available In precursors for ALD growth with H_2S. Unsatisfied, we synthesized a new In precursor and explored its potential for In_2S_3 growth by ALD. With the newly synthesized precursor and 1 wt % H_2S as the S source, we obtain amorphous or polycrystalline thin films with a growth rate up to 0.89 Å/cycle. The novel metal organic precursor is exceedingly stable, up to ~300 °C, yet exhibits good reactivity with −SH terminated surfaces at temperatures as low as 125 °C. Films grown at 200 °C exhibit precisely the stoichiometry of In_2S_3 within error and show properties consistent with material largely free from impurities.

■ EXPERIMENTAL SECTION

General Consideration. All chemical manipulations were carried out using standard Schlenk and glovebox techniques in a nitrogen atmosphere. Pentane and diethyl ether were dried by passing through two columns (one neutral alumina column and one copper(II) oxide-Q5 column for pentane and two neutral alumina for diethyl ether), stored over 4 Å molecular sieves and tested periodically with sodium benzophenone ketyl. Celite and molecular sieves were kept above 150 °C for a minimum of 5 days and were heated to 160 °C under reduced pressure overnight prior to use. *N,N*′-Diisopropylcarbodiimide (99%) and $In(Cl)_3$ (98%) were used as received from Sigma-Aldrich, while methyl lithium (1.57 M in diethyl ether) was used as received from Alfa Aesar. ^1H (300 MHz) and ^{13}C (75 MHz) NMR spectra were recorded on a Bruker Avance 300 MHz instrument at ambient temperature. Chemical shifts were referenced to internal protio solvent peaks. NMR solvent was purchased from Cambridge Isotopes and dried over 4 Å molecular sieves for a minimum of 48 h prior to use.

Synthesis of In(III) *N,N*′-Diisopropylacetamidinate [In-(amd)$_3$]. A 250 mL round-bottom flask was charged with a Teflon stir bar, 9.0 mL (57.5 mmol) of diisopropylcarbodiimide, and 150 mL of diethyl ether. The mixture was cooled to −30 °C, and then 35.9 mL (57.4 mmol) of 1.57 M MeLi was added dropwise in two portions. After allowing the reaction to warm to room temperature, it was stirred for a total time of ca. 2 h. After the reaction was cooled to −30 °C, 4.246 g of $InCl_3$ (19.2 mmol) was slowly added as a solid. The white, cloudy reaction was allowed to proceed overnight at room temperature (ca. 16 h), and then volatiles were removed under reduced pressure. The resulting white solid was dissolved in 100 mL of pentane, filtered through a Celite plug, and the plug washed (3 × 20 mL pentane). The clear and colorless solution was evaporated under reduced pressure at room temperature to produce 9.371 g (17.40 mmol) of a white flakey solid in a 91% yield. This procedure produces pure $In(amd)_3$ (by ^1H NMR spectroscopy, shown in Supporting Information Figures SI1 and SI2) from pure starting material. However, further purification is possible by dissolving the solid isolated from filtration in a minimum amount of pentane, allowing the mixture to cool to −30 °C, and collecting and washing the white crystalline material (3 × 2 mL pentane). Further purification can alternatively be performed by sublimation at 150 °C and 20 mTorr. A melting point was not observed up to 320 °C, when the material turned brown (decomposition). ^1H NMR (300 MHz, C_6D_6) spectrum peaks (Figure S1): δ 3.63 (6H, N*CH*$(CH_3)_2$, septet, J_{CH} 6.3 Hz), 1.62 (9H, amidinate *CH*$_3$, singlet), 1.35 (18H, NCH(*CH*$_3$)$_2$, doublet, J_{CH} 6.3 Hz), 1.18 (18H, NCH(*CH*$_3$)$_2$, doublet, J_{CH} 6.3 Hz). ^{13}C NMR (75.4 MHz, C_6D_6, ppm) spectrum peaks (Figure S2): δ 164.56 (N_2CCH_3), 47.44 (amidinate *CH*$_3$), 26.43 and 25.17 (NCH(*CH*$_3$)$_2$), 11.46 (N*CH*$(CH_3)_2$).

In_2S_3 films were grown in a commercial hot-wall ALD tool (Savannah 200, Cambridge NanoTech) adapted for compatibility with H_2S.[30] A constant 10 sccm stream of ultrahigh purity nitrogen carrier/purge gas is continuously pumped through the tool resulting in a base pressure of 0.25 Torr. $In(amd)_3$ was delivered under its own vapor pressure (without nitrogen assist) from a 50 cm^3 stainless steel cylinder heated to 190 °C. Note that $In(amd)_3$ actually sublimes well below this temperature (20 mTorr at 150 °C in a round-bottom flask). However, the small precursor surface area in its cylinder requires a higher temperature to volatilize enough material for saturating growth. A dilute hydrogen sulfide mixture (1% in N_2, Matheson Tri-Gas) was stepped down to 500 Torr through a two-stage regulator before flowing through a 300 μm pinhole just prior to the pneumatic ALD valve. One growth cycle consists of four sequential steps: a 4 s $In(amd)_3$ dose (~0.04 Torr partial pressure), 25 s purge, a 0.3 s H_2S dose (~0.45 Torr partial pressure), and 25 s purge. This sequence, denoted 4−25−0.3−25, was repeated throughout unless otherwise noted. Growth was explored with a range of reactor temperatures from 140 to 240 °C. Note that spectral ellipsometry on Si wafers confirms that no CVD or condensation of $In(amd)_3$ occurs at 140 °C or higher.

The possibility of ALD processes for In_2S_3 that utilize several commercially available In precursors was also explored under similar conditions. These precursors and their required volatilization temperature in our tool are cyclopentadienyl indium (99.99% from Strem, 70 °C), trimethylindium (98+% from Strem, 45 °C), tris(2,2,6,6-tetramethyl-3,5-heptanedionatio)indium(III) (99% from Strem, >190 °C), indium(III) acetylacetonate (99.99% from Sigma-Aldrich, >190 °C), and an indium tris(guanidinate) (synthesized using a previously reported method from the literature, 160 °C).[31] Deposition attempts for each precursor with sufficient and sustainable volatility were performed under a range of conditions including reactor temperatures from 150 to 250 °C, precursor pulse lengths from 0.1 to 5 s, and H_2S pulse lengths from 0.015 to 1 s. For precursors with low volatility, multiple pulses per cycle (with sufficiently long purge times between pulses) were required to increase exposure time.

Quartz crystal microbalance (QCM) measurements were performed with a modified reactor lid wherein mass changes may be monitored in situ directly adjacent to and simultaneous to ex situ film growth as previously described.[32] The lid has two QCMs on a line between the reactor inlet and outlet. The “Front QCM” and “Back QCM” lie 5.1 and 15.2 cm downstream of the precursor inlet, respectively. Films for ex situ analysis were grown on Si(100) substrates with native oxide as well as fused quartz. Films discussed in this Article were grown ~10 cm from the inlet. Prior to growth, substrates were subjected to 10 min of acetone sonication, rinse, 10 min of isopropanol sonication, rinse, a N_2 blast dry, and 10 min in the tool to equilibrate temperature. Nanoscale film morphology was determined via scanning electron microscopy (SEM, Hitachi S-4700) and atomic force microscopy (AFM, Asylum MFP-3D). The crystallinity and crystalline orientation of In_2S_3 films on fused quartz were determined by X-ray diffraction (XRD, Cu Kα radiation, Rigaku Miniflex Plus). Absorption studies were performed using a Cary 5000 UV−vis-NIR from Agilent Technologies including an integrating sphere to correct for sample reflectivity. The majority carrier type, composition, and mobility were investigated with a Hall measurement system (HMS-3000, Ecopia) at room temperature. The absolute film composition and impurity incorporation was determined by Rutherford backscattering spectroscopy (RBS) and depth-profiling Auger spectroscopy, both performed by Evans Analytical. Film thickness, density, and roughness were determined by X-ray reflectivity (XRR, Philips X'Pert Pro MRD diffractometer, Cu Kα radiation). XRR data were fit using the Abeles Matrix method within the Motofit software package.[33]

■ RESULTS AND DISCUSSION

Prior to the synthesis of $In(amd)_3$, a number of commercially available In precursors were explored. ALD processes for each were found unsatisfactory for the reasons summarized briefly below. Trimethylindium is a high volatility precursor that has been utilized for ALD growth of In_2O_3 using H_2O with limited success[34,35] and, more recently with N_2O.[36] Unfortunately, no growth was observed when pulsed sequentially with H_2S between 150 and 250 °C. Cyclopentadienyl indium, which has previously been used with ozone for the ALD of In_2O_3,[37] also failed to produce sustainable growth of In_2S_3 in concert with H_2S. Cyclopentadienyl ligands are often difficult to remove and in this case, direct evidence is available from mechanistic studies of ALD with sequential H_2O and O_2 exposure.[38] Other In precursors failed primarily because only modest vapor pressure and/or evaporation rates were achievable at temperatures less than that at which the precursor decomposes. $In(acac)_3$ has been successfully delivered with nitrogen assist, but its propensity for thermal decomposition has been previously noted.[29] Saturating doses could not be readily achieved without nitrogen assist near the decomposition temperature of 150 °C. Tris(2,2,6,6-tetramethyl-3,5-heptanedionato)indium(III) [In-$(TMHD)_3$] was also explored, but was, as expected, found to be less volatile than $In(acac)_3$. An indium guanidinate, $In[(N^iPr)_2CNMe_2]_3$, was also synthesized based on previous reports.[31] Although ALD growth was observed, sufficient precursor delivery was not achieved below 110 °C, the temperature at which this precursor decomposes significantly.[31] In contrast, the new $In(amd)_3$ precursor provides ample precursor delivery without nitrogen assist at 190 °C, below the precursor decomposition temperature (>300 °C) and standard ALD valve limit (200 °C). The molecular structure of the new In(III) precursor is shown in Figure 1.

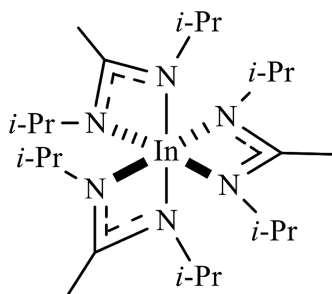

Figure 1. Molecular structure of In(III) *N,N′*-diisopropylacetamidinate.

Facile synthesis of $In(amd)_3$ is conveniently performed on the multigram scale to produce an off-white solid with minimum purification. First, synthesis of the lithium salt of the desired acetamidinate from methyl lithium and the carbodiimide is performed,[39,40] followed by salt metathesis of that reaction mixture with indium(III) chloride. While there is not a large amount of literature on the synthesis or reactivity of amidinate compounds of indium(III),[41] Richeson and Zhou synthesized the tris-*N,N′*-dicyclohexylacetimidinate of indium and observed two sets of peaks for the three acetimidinate ligands in room temperature ^1H NMR, consistent with a C_2 symmetric In center;[42] a pattern we also observe for $In(amd)_3$, where two equivalent doublets are observed at 1.35 and 1.18 ppm (Figure S1). Thermal investigation of this product shows that the compound cleanly sublimes at 150 °C and 20 mTorr and exhibits stability up to ca. 320 °C in a sealed vessel, when it turned a dark brown and became ^1H NMR silent. The large temperature span between sublimation temperature (150 °C) and decomposition temperature (>300 °C) makes $In(amd)_3$ unique among In(III) precursors for its utility in chemical vapor and atomic layer deposition.

Having established a large window of precursor stability, the self-limiting nature of each half-reaction was investigated at a 200 °C reactor temperature with the $In(amd)_3$ source held at 190 °C. The total exposure of $In(amd)_3$ and H_2S was varied by systematically increasing the length of time to which the reaction chamber was open to each precursor source. Under the conditions employed, a relatively constant partial pressure (~0.04 Torr) was produced for the duration of the $In(amd)_3$ pulse. The growth rate is reported as the average mass per square centimeter per cycle over 50 cycles measured by QCM, Figure 2.

Saturating growth behavior is observed after an ~4 s (0.15 Torr·s) dose of $In(amd)_3$, with no additional growth after at least a 3× greater exposure. The half-reaction with H_2S also displays a saturating reaction, in this case with a dose of less than 0.4 s (13 Torr·s), likely due to the significantly larger partial pressure of the compressed H_2S gas. Together these experiments demonstrate the strictly self-limiting nature of this new ALD process. Systematic variation of the wait time between each precursor pulse indicates that purge times as short as 5 s at 200 °C prevent gas-phase mixing (CVD) or reaction of physisorbed species. For purge times down to 5 s, the increase in growth rate is within 10% of purge times up to 50 s, Figure S3.

One hypothetical mechanism for the sequential surface reactions of $In(amd)_3$ with surface −SH groups and H_2S is presented as eqs 1 and 2:

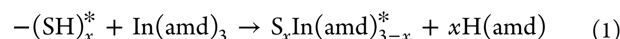

$$-(SH)_x^* + In(amd)_3 \rightarrow S_xIn(amd)_{3-x}^* + xH(amd) \quad (1)$$

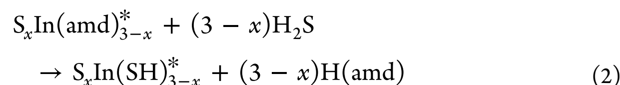

$$S_xIn(amd)_{3-x}^* + (3-x)H_2S \rightarrow S_xIn(SH)_{3-x}^* + (3-x)H(amd) \quad (2)$$

where the asterisk (*) denotes a surface species. This reaction mechanism is in close analogy to the hydroxyl mechanism observed in many oxide ALD processes, including trimethylaluminum (TMA) and water.[15] While no chemically sensitive probes have been utilized in this study, we note that similar mechanisms have been deduced for sulfides deposited with $In(acac)_3$[13] and hexakis(dimethylamido)digallium ($Ga_2(NMe_2)_6$).[43] The latter article provides FTIR evidence for a sulfhydryl mechanism, and both systems exhibit the same decreasing growth rate with temperature. The repetition of these reactions in an ABAB... sequence leads to In_2S_3 growth in an atomic layer-by-layer fashion. Ideally, after one total ALD cycle, that is, reactions 1 and 2, has occurred, all of the amidinate ligands will have been removed, leaving no residual light elements. This statement is supported by the lack of C, N, or O impurity as deduced from ex situ analysis (see below). The variable x may then be solved for by examining the mass change in each half cycle relative to that of the overall mass change per cycle. In situ QCM measurements at 200 °C are shown Figure 3 using standard cycle timing.

Under these conditions, growth at both QCMs tracks very closely, yielding an overall growth rate of 19 ± 3 ng/cycle. The details of each half-cycle (Figure 3b) reveal a large mass gain (Δm_1) upon exposure to $In(amd)_3$. This relatively rapid and

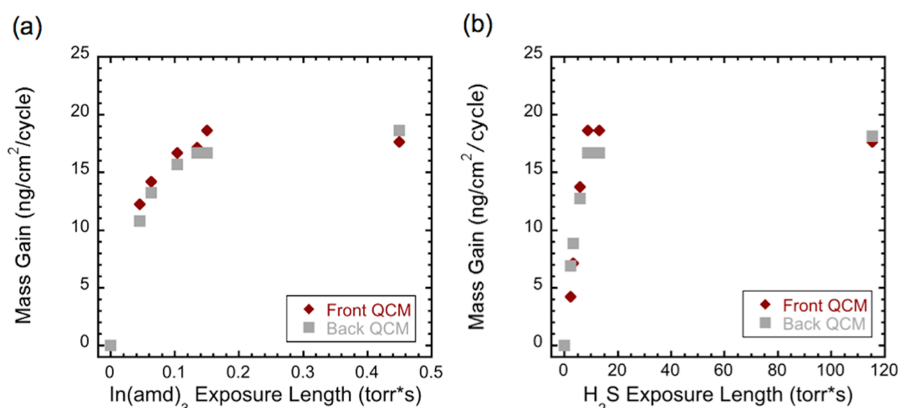

Figure 2. Mass gain as a function of precursor exposure time for (a) $In(amd)_3$ (x−25−0.3−25) where x = 0.5, 1, 2, 3, 4, and 12 s, and (b) H_2S (4−25−y−25) where y = 0.05, 0.1, 0.2, 0.3, 0.4, and 0.5 s. The 12 s $In(amd)_3$ pulse is achieved through three consecutive 4 s doses separated by 50 s to allow sufficient time for vapor equilibration over the solid precursor.

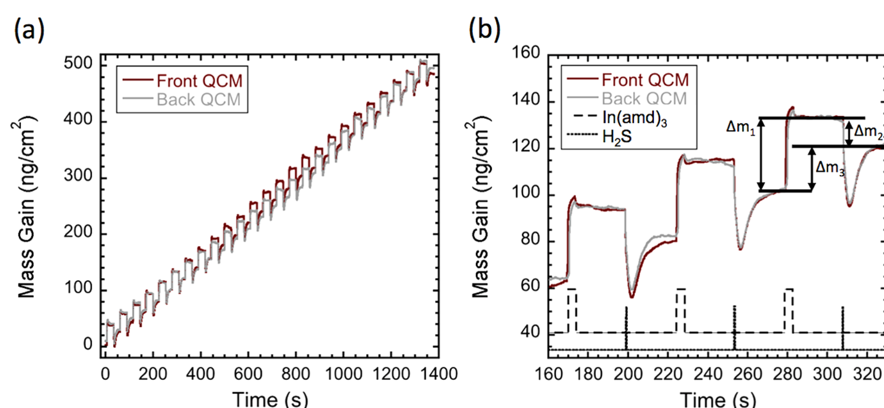

Figure 3. (a) Mass deposited as a function of time upon sequential dosing of $In(amd)_3$ and H_2S. The pulse sequence is 4−25−0.3−25. (b) A high-resolution trace reveals abrupt mass changes coincident with precursor exposure.

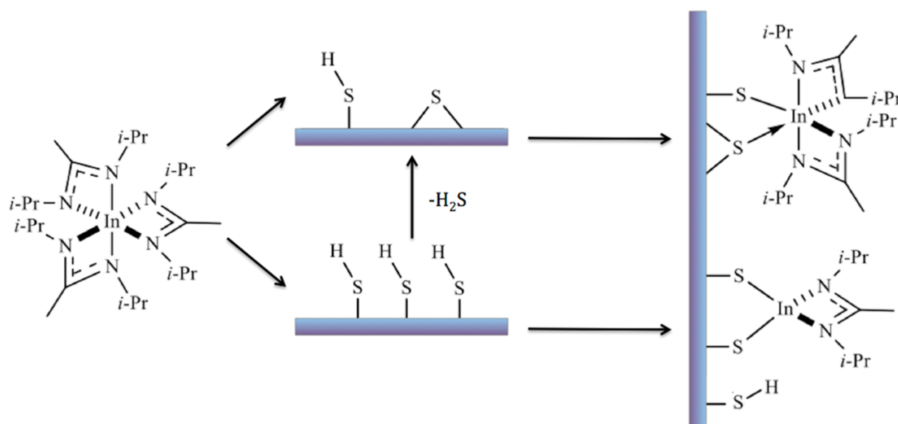

Figure 4. Idealized schematic of $In(amd)_3$ reacting with adjacent SH/S sites and two SH sites during the $In(amd)_3$ half reaction.

large mass gain (32 ± 2 ng/cm^2) is consistent with the facile reaction of the In precursor and retention of a fragment that includes In. Upon exposure of this surface to H_2S, a transient is recorded in response to the large pressure swing and/or local heating to which the quartz crystals are also sensitive. After equilibration, a mass loss (Δm_2) of 13 ± 2 ng is observed, consistent with replacement of the bulky amidinate ligand with a significantly lighter −SH group. By reconciling the above equations with the mass changes, we conclude that the ratio of overall formula unit addition ($\Delta m_3 = InS_{1.5} = 163$) to addition of the first step (Δm_1 = In + (3 − x)(amd) − xH = 454 − 114x) should be identical to the mass change observed in Figure 2 (19/32). Solving for x reveals that in the mechanism hypothesized on average 1.6 ± 0.3 ligands would be lost in the first step and 1.4 ± 0.3 upon exposure to H_2S. However, further study is required to provide firm evidence for the proposed mechanism.

A reaction scenario consistent with these results is as follows: an equilibrium distribution of surface −SH and bridging surface S groups may exist after H_2S exposure (Figure 4). When the In

complex reacts with this surface, it has the possibility of reacting with adjacent SH and S groups as well as two adjacent SH groups. The reaction with each site may produce different surface species in which either one or two ligands are lost, respectively. The subsequent H_2S pulse may then remove the remaining amidinate ligands from both species and reset the surface to its equilibrium concentration of SH and bridging S groups.

If this is the case, and surface SH density contributes to overall $In(amd)_3$ reaction with the surface, then the growth rate should show the large and saturating dependence on H_2S concentration that we observe experimentally, see Figure 2b. Furthermore, significant dependency of the growth rate on temperature might be expected as influenced by the equilibrium concentration of SH and bridging S groups at each temperature. A very similar mechanism is suggested for GaS_x deposition, where the decreasing growth rate with increasing temperature is attributed to smaller −SH coverages (based on QCM data).[43] Figure 5 shows the effect of reactor temperature on growth rate over a range greater than 100 °C.

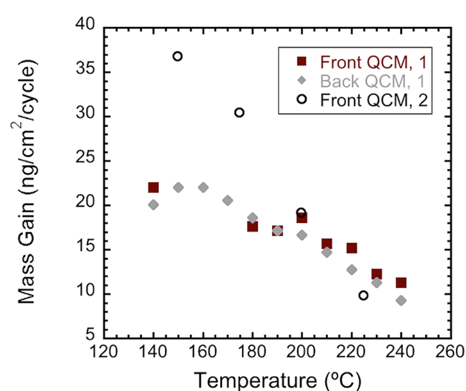

Figure 5. Growth per cycle decreases as a function of reactor temperature. The pulse sequence for all temperatures is 4−30−0.3−30. QCM results labeled (1) are grown with 1% H_2S in N_2, while results labeled (2) are observed when employing a more concentrated, 4% H_2S in N_2.

Initially, process conditions optimized at 200 °C (see Figure 2) are applied such that the same amount of $In(amd)_3$ and H_2S is pulsed into the reactor at each temperature. An apparent growth rate plateau is observed between 140 and 170 °C, and the rate then steadily decreases with increasing temperatures up to 240 °C (maroon squares and gray diamonds). The observed plateau occurs because cool temperatures appear to exhibit intrinsically greater growth rates per cycle, but do not fully saturate under pulse conditions optimized at 200 °C. Increasing the amount of H_2S in each pulse by a factor of 4 (black open circles) allows for full saturation, and reveals much larger growth rates at lower temperatures. The linear decrease in growth rate per cycle with increasing substrate temperature, now clearly visible, has been seen with other indium ($In(acac)_3$),[13] zinc,[44] gallium,[43] and tin sulfides.[45] In some of these systems, the effect was attributed to recombinative desorption of H_2S at higher temperatures (see vertical arrow in Figure 4),[45] thus adding further weight to the mechanism offered herein, eq 1 and 2. In this proposed scenario, the growth rate per cycle is reduced due to a lower density of $In(amd)_3$ binding sites as governed by the surface density of bridging S groups that result from two formerly SH sites; see again Figure 4.

Thin films were grown on fused quartz substrates for ex situ characterization according to the process conditions gleaned from the in situ studies detailed above. Dense, well adhered, and specular thin films were obtained that show the characteristic orange color of a ∼2.0 eV band gap material. The microstructure of In_2S_3 films deposited at several temperatures was investigated by SEM, Figure 6.

All films appear uniform over the ∼3 cm^2 substrate, with no sign of pinholes or cracks. Thin films deposited at 150 °C exhibit the rounded and random structure typically observed in largely amorphous materials. In contrast, growth at higher temperatures exhibits the characteristically sharp edges of polycrystalline films, with the apparent grain size increasing from ∼50 to ∼250 nm as the growth temperature increases from 175 to 225 °C. This result differs from the reports of ALD In_2S_3 films grown with $In(acac)_3$ where no major increase in grain size (typically 10−25 nm) is observed, only the variation of grain size decreases with increasing temperature.[14,26] EDS data confirms the presence of both principal elements and further reveals a constant ratio of In:S for films grown between 150 and 225 °C, Figure S4. AFM images show similar structures for films grown on fused quartz, Figure S5. At 150 °C, films have rounded and random features, while films grown at 225 °C have sharp edges and the same trigonal structures observed with SEM images of In_2S_3 on Si.

The crystallinity of In_2S_3 films grown by the new ALD process was confirmed by the Θ−2Θ XRD scans shown in Figure 7.

As-deposited films at 150 °C are largely amorphous, showing only a hint of the expected reflections with our benchtop diffractometer. Films grown at 175 °C and above show clear and sharp reflections that can be indexed to the β-In_2S_3 crystal structure (JCPDS 25-0390).[46] This tetragonal crystal structure is expected for In in the 3+ oxidation state at a growth temperature above 115 °C[47] and has been previously observed for In_2S_3 deposited by ALD[12−14,27] among other methods. Sharper peaks are observed at higher temperature, indicative of larger grain size in corroboration with SEM analysis. All crystalline thin films showed significant texture, as evident by absent reflections. The dominance of the (103) series indicates that these crystalline planes are primarily aligned parallel to the surface. A small fraction of (109) reflections are also observed at 175 and 200 °C but are absent at 225 °C.[48]

Elemental concentrations were determined by Rutherford backscattering spectroscopy (RBS) and depth-profiling Auger electron spectroscopy (AES), Figures S6 and S7, respectively) on films grown at 200 °C. RBS confirms that indium and sulfur have the expected stoichiometric ratio of 40%/60%. AES showed no sign of carbon, oxygen, or nitrogen in the bulk of sulfide films down to an estimated detection limit of 1%, 0.5%, and 4%, respectively. The modest detection limit for N is due to peak overlap with the large In signal. Oxygen and carbon contamination were only present in a thin surface layer above the bulk In_2S_3 film as deduced by depth profiling (see Figure S7). Glow discharge optical emission spectroscopy (GDOES) measurements show no measurable amount of Li (data not shown), which is present during $In(amd)_3$ synthesis. EDS and X-ray fluorescence (XRF) results confirm that films grown at different temperatures have the same In/S ratio and reveal no obvious impurities.

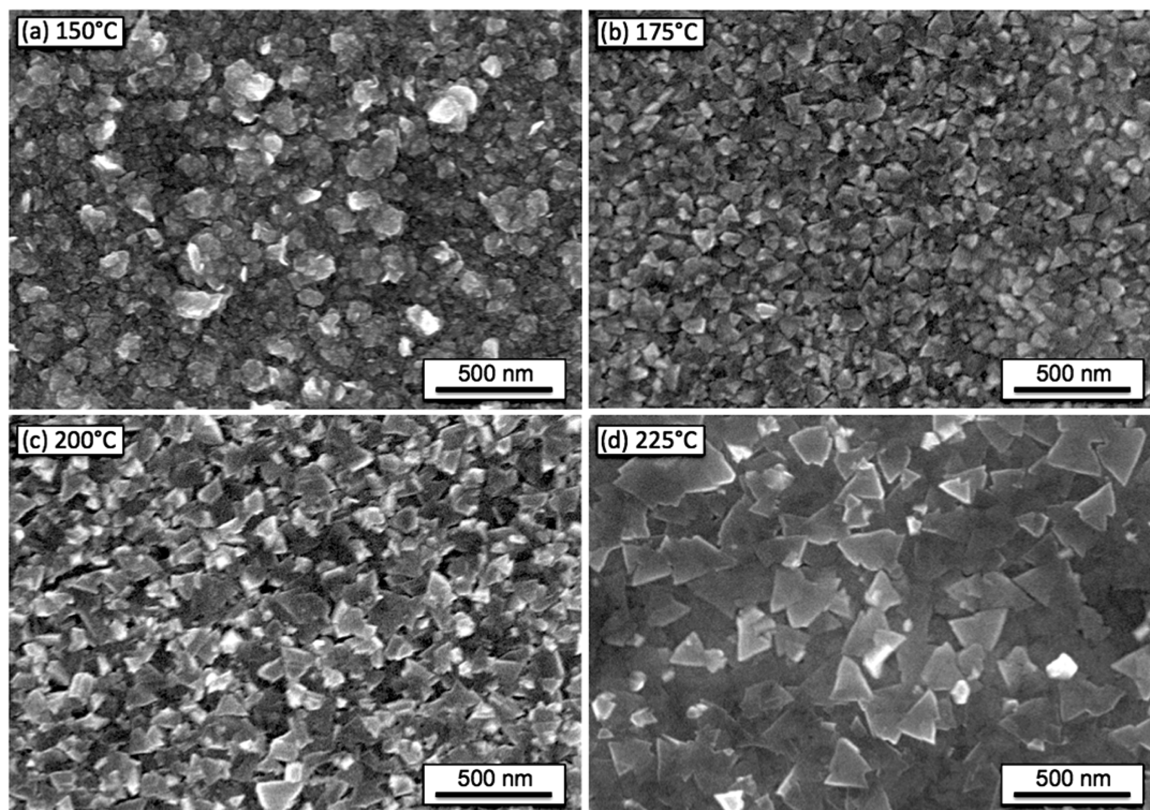

Figure 6. SEM images at 50 000× magnification for In_2S_3 films grown on Si(100) at (a) 150 °C, (b) 175 °C, (c) 200 °C, and (d) 225 °C. The thicknesses for these films are as follows: 150 °C, 102 nm; 175 °C, 98 nm; 200 °C, 83 nm; and 225 °C, 82 nm.

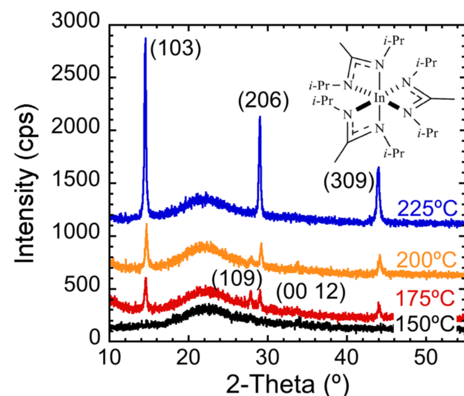

Figure 7. X-ray diffraction from In_2S_3 films grown on fused quartz. Traces have been offset for clarity. The thicknesses for these films are as follows: 150 °C, 102 nm; 175 °C, 98 nm; 200 °C, 83 nm; and 225 °C, 82 nm.

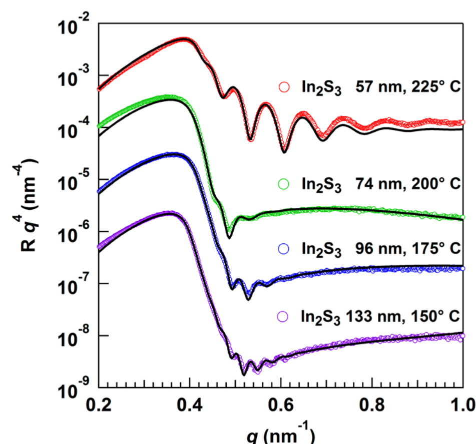

Figure 8. X-ray reflectivity data and fits (black lines) for In_2S_3 films grown on fused quartz at 150 (purple), 175 (blue), 200 (green), and 225 °C (red).

Film thickness (t), roughness (σ), and density (ρ) were determined for a batch of In_2S_3 films grown on fused quartz using X-ray reflectivity, Figure 8, using a single layer model for the In_2S_3 film. The data is plotted as the reflected intensity (R) times q^4 as a function of q, where $q = 4\pi \sin(\Theta)/\lambda$ and λ is the X-ray wavelength. The q^4 factor compensates for the $R \propto q^{-4}$ drop in reflected intensity at q values larger than the critical angle and allows for better visualization of the relatively small Kiessig fringes that arises due to the In_2S_3 thin film overlayer.

The XRR fitting results are reported in Table 1. Uncertainties for each result are reported with 95% confidence intervals derived from χ^2 maps for each fit parameter. At the temperatures which polycrystalline thin films are observed (Figure 8), we find an In_2S_3 film density that is , on average, slightly lower (∼3%) than the bulk density of β-In_2S_3 (4.61 g/cm^3)[46] but consistently higher than XRR-derived densities previously reported for In_2S_3 ALD films (4.31 g/cm^3).[13] From this data, we calculate an average growth of 0.40 Å/cycle at 200 °C and a corresponding mass deposition rate of 19 ng/cycle at 200 °C. Thus, the growth rate as derived from ex situ film studies precisely matches that measured in situ via QCM under the same process conditions (see Figures 3 and 4). The amorphous film grown at 150 °C is determined to have a slightly lower density (4.15 g/cm^3) that allows calculation of the growth rate from the QCM-determined mass deposited

Table 1. XRR-derived t, σ, ρ Values Acquired from Fits Presented in Figure 8[a]

T	χ^2	t (nm)	σ (nm)	ρ (g/cm^3)
150 °C	2.21	133^{+6}_{-8}	$6.5^{+0.3}_{-0.3}$	$4.15^{+0.09}_{-0.14}$
175 °C	1.57	96^{+6}_{-5}	$6.5^{+0.4}_{-0.3}$	$4.47^{+0.13}_{-0.14}$
200 °C	5.60	74^{+4}_{-4}	$7.5^{+0.4}_{-0.4}$	$4.51^{+0.14}_{-0.14}$
225 °C	4.82	57^{+1}_{-1}	$3.8^{+0.2}_{-0.3}$	$4.47^{+0.09}_{-0.09}$

[a] $\chi^2 = (N - N_p)^{-1}\Sigma_k((I_{meas,k} - I_{calc,k})^2/Err_k^2)$, where $I_{meas,k}$ and $I_{calc,k}$ are the measured and calculated intensities of the kth data point, respectively. Err_k is the uncertainty for the data point, and N and N_p represent the total number of data points and fitting parameters, respectively. Error bounds define the 95% confidence interval for each parameter.

each cycle to be: 0.89 Å/cycle. This ample growth per cycle, the largest reported to date for halide-free In_2S_3 ALD, corroborates the apparently facile surface chemistry of this ALD process.

The optical absorption coefficient as a function of photon energy was obtained from reflection-corrected optical absorbance spectroscopy for several growth temperatures, Figure 9.

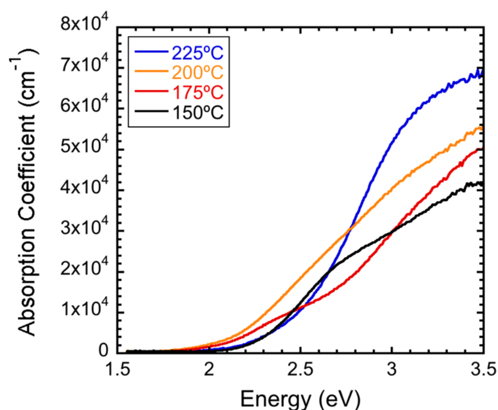

Figure 9. Absorption coefficient data for In_2S_3 films grown on fused quartz at 150 °C (black), 175 °C (red), 200 °C (orange), and 225 °C (blue). The thicknesses for these films are as follows: 150 °C, 102 nm; 175 °C, 98 nm; 200 °C, 83 nm; and 225 °C, 82 nm.

The onset of absorbance was found to be between 1.9 and 2.0 eV and independent of deposition temperature. The band gap of In_2S_3 is notoriously difficult to characterize, with reports varying between 1.9 and 2.8 eV for β-In_2S_3 alone. The issue is further clouded by debate about the direct or indirect nature of the band gap.[1,49] Recent density functional theory (DFT) studies suggests that the lowest energy gap is indirect for β-In_2S_3, but a slightly larger direct gap transition also exists.[49] The tetragonal crystal structure of β-In_2S_3 also has two distinct axes (a/b and c), which is predicted to lead to significant optical anisotropy near the absorption edge. Among these films, we see evidence for the three DFT-calculated absorption peaks, 2.3 eV (a/b), 2.75 eV (c), and 3.0 eV (a/b), that were also reported.[49] However, at this point, a quantitative deconvolution of the spectral components as a function of film orientation to corroborate (or not) the DFT simulations is not viable.

The electronic properties of ALD-grown films were elucidated via Hall measurement as a function of growth temperatures, Figure 10. All films show clear n-type conductivity as-deposited with the exception of 150 °C films, which were too resistive to quantify.

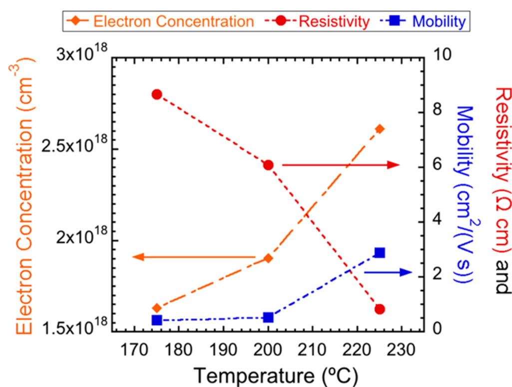

Figure 10. In_2S_3 films show n-type conductivity in proportion to the electron mobility and concentration. The thicknesses for these films are as follows: 175 °C, 98 nm; 200 °C, 83 nm; and 225 °C, 82 nm.

Typical mobilities are near 0.5 cm^2/(V·s) for films grown at or below 200 °C, but increase almost an order of magnitude to 3 cm^2/(V·s) for films grown at 225 °C. These values position ALD-grown In_2S_3 thin films as an interesting electronic material that compares well to In_2S_3 thin films grown by other methods.[50,51] Like most polycrystalline films, these value fall short of bulk single crystal mobilities, which are reported to reach 200 cm^2/(V·s).[52] A relatively constant carrier concentration is observed near ∼2 × 10^{18} cm^{-3} at all growth temperatures. This is an order of magnitude higher than that of films produced from the $In(acac)_3$ ALD process (10^{16}–10^{17} cm^{-3}),[14] but significantly lower than carrier concentrations reported for In_2S_3 films grown by some other methods.[50,52] For undoped In_2S_3 films, the intrinsic donors are sulfur vacancies[53] and indium interstitials.[52,53] These electronic properties suggest that growth with $In(amd)_3$ forms more of these sites than growth with $In(acac)_3$, giving higher carrier concentrations. It is also likely in $In(acac)_3$ grown films (given their large deficiency of S)[13,22] that these donor sites are reduced by oxygen incorporation in the films.[51] The overall effect of growth temperature is an order of magnitude increase in conductivity that tracks the increasing mobility and charge carrier concentration with increasing growth temperature. The increasing grain/crystal sizes with temperature could explain the improved mobility and conductivity.

CONCLUSIONS

A facile and rapid atomic layer deposition process for indium sulfide was demonstrated by employing a new indium(III) amidinate precursor. Optimization of process conditions allows for the deposition of very low-impurity thin films over a nearly 100 °C ALD window (from 150 to 225 °C). A maximum growth rate of 0.89 Å/cycle was observed at 150 °C and steadily decreased to 0.22 Å/cycle at 225 °C. Films grown at 175 °C or higher were shown to be largely (103) oriented β-In_2S_3 as deposited. Elemental analysis of the thin films reveals indium and sulfur in precise 2:3 atomic ratio and no sign of oxygen, nitrogen, carbon, or halogen impurities in the bulk thin film. An optical absorbance onset revealed the expected band gap near 2.0 eV with absorption coefficients that vary slightly with film orientation. An analysis of the electronic properties as a function of growth temperature reveals mobilities in excess of 1 cm^2/(V·s).

ASSOCIATED CONTENT

Supporting Information

^{1}H NMR and ^{13}C NMR spectra of indium(III) amidinate, ALD purge length studies for In(amd)$_3$ and H_2S, EDS of In_2S_3 films deposited at multiple temperatures, RBS data for In_2S_3 deposited at 200 °C, and AES for the same films. This material is available free of charge via the Internet at http://pubs.acs.org.

AUTHOR INFORMATION

Corresponding Author

*E-mail: martinson@anl.gov.

Notes

The authors declare no competing financial interest.

ACKNOWLEDGMENTS

Argonne National Laboratory's work was supported under U.S. Department of Energy contract DE-AC02-06CH11357. The electron microscopy was accomplished at the Electron Microscopy Center at Argonne National Laboratory, a U.S. Department of Energy Office of Science Laboratory operated under Contract No. DE-AC02-06CH11357 by UChicago Argonne, LLC. M.S.W. would like to thank the Department of Education GAANN Fellowship under grant #P200A090137. We also wish to thank Dr. Shannon C. Riha for useful discussions and Paul A. Fenter for access to the atomic force microscope. A.S.H. would like to thank the Department of Energy and the Illinois Institute of Technology for funding and startup support.

REFERENCES

(1) Naghavi, N.; Abou-Ras, D.; Allsop, N.; Barreau, N.; Bucheler, S.; Ennaoui, A.; Fischer, C. H.; Guillen, C.; Hariskos, D.; Herrero, J.; Klenk, R.; Kushiya, K.; Lincot, D.; Menner, R.; Nakada, T.; Platzer-Bjorkman, C.; Spiering, S.; Tiwari, A. N.; Torndahl, T. Buffer Layers and Transparent Conducting Oxides for Chalcopyrite Cu(In,Ga)-(S,Se)$_2$ Based Thin Film Photovoltaics: Present Status and Current Developments. *Prog. Photovoltaics* **2010**, *18*, 411−433.

(2) Hariskos, D.; Spiering, S.; Powalla, M. Buffer Layers in Cu(In,Ga)Se$_2$ Solar Cells and Modules. *Thin Solid Films* **2005**, *480*, 99−109.

(3) Lucena, R.; Aguilera, I.; Palacios, P.; Wahnon, P.; Conesa, J. C. Synthesis and Spectral Properties of Nanocrystalline V-Substituted In_2S_3, a Novel Material for More Efficient Use of Solar Radiation. *Chem. Mater.* **2008**, *20*, 5125−5127.

(4) Ho, C. H. Enhanced Photoelectric-Conversion Yield in Niobium-Incorporated In_2S_3 with Intermediate Band. *J. Mater. Chem.* **2011**, *21*, 10518−10524.

(5) Hariskos, D.; Ruckh, M.; Ruhle, U.; Walter, T.; Schock, H.; Hedstrom, J.; Stolt, L. A Novel Cadmium Free Buffer Layer for Cu(In,Ga)Se$_2$ Based Solar Cells. *Sol. Energy Mater. Sol. C* **1996**, *41−2*, 345−353.

(6) Asenjo, B.; Chaparro, A.; Gutierrez, M.; Herrero, J.; Maffiotte, C. Quartz Crystal Microbalance Study of the Growth of Indium(III) Sulphide Films from a Chemical Solution. *Electrochim. Acta* **2004**, *49*, 737−744.

(7) Trigo, J.; Asenjo, B.; Herrero, J.; Gutierrez, M. Optical Characterization of In_2S_3 Solar Cell Buffer Layers Grown by Chemical Bath and Physical Vapor Deposition. *Sol. Energy Mater. Sol. Cells* **2008**, *92*, 1145−1148.

(8) Amin, N.; Hossain, M. I.; Hamzah, N. R.; Chelvanathan, P. Physical and Optical Properties of In_2S_3 Thin Films Deposited by Thermal Evaporation Technique for CIGS Solar Cells. *IEEE First Conf. Clean Energy Technol. CET* **2011**, *1*, 63−67.

(9) Allsop, N.; Schonmann, A.; Belaidi, A.; Muffler, H.; Mertesacker, B.; Bohne, W.; Strub, E.; Rohrich, J.; Lux-Steiner, M.; Fischer, C. Indium Sulfide Thin Films Deposited by the Spray Ion Layer Gas Reaction Technique. *Thin Solid Films* **2006**, *513*, 52−56.

(10) Allsop, N.; Hansel, A.; Visbeck, S.; Niesen, T.; Lux-Steiner, M.; Fischer, C. The Dry and Damp Heat Stability of Chalcopyrite Solar Cells Prepared with an Indium Sulfide Buffer Deposited by the Spray-ILGAR Technique. *Thin Solid Films* **2006**, *511*, 55−59.

(11) Wang, S. S.; Shiou, F. J.; Tsao, C. C.; Huang, S. W.; Hsu, C. Y. An Evaluation of the Deposition Parameters for Indium Sulfide (In_2S_3) Thin Films using the Grey-Based Taguchi Method. *Mater. Sci. Semicond. Process.* **2013**, *16*, 1879−1887.

(12) Asikainen, T.; Ritala, M.; Leskela, M. Growth Of In_2S_3 Thin-Films by Atomic Layer Epitaxy. *Appl. Surf. Sci.* **1994**, *82−3*, 122−125.

(13) Sarkar, S. K.; Kim, J. Y.; Goldstein, D. N.; Neale, N. R.; Zhu, K.; Elliot, C. M.; Frank, A. J.; George, S. M. In_2S_3 Atomic Layer Deposition and Its Application as a Sensitizer on TiO_2 Nanotube Arrays for Solar Energy Conversion. *J. Phys. Chem. C* **2010**, *114*, 8032−8039.

(14) Naghavi, N.; Henriquez, R.; Laptev, V.; Lincot, D. Growth Studies and Characterisation of In_2S_3 Thin Films Deposited by Atomic Layer Deposition (ALD). *Appl. Surf. Sci.* **2004**, *222*, 65−73.

(15) George, S. M. Atomic Layer Deposition: An Overview. *Chem. Rev.* **2010**, *110*, 111−131.

(16) Suntola, T. Cost-Effective Processing by Atomic Layer Epitaxy. *Thin Solid Films* **1993**, *225*, 96−98.

(17) Riha, S.; Racowski, J.; Lanci, M.; Klug, J.; Hock, A.; Martinson, A. Phase Discrimination through Oxidant Selection in Low-Temperature Atomic Layer Deposition of Crystalline Iron Oxides. *Langmuir* **2013**, *29*, 3439−3445.

(18) van Delft, J.; Garcia-Alonso, D.; Kessels, W. Atomic Layer Deposition for Photovoltaics: Applications and Prospects for Solar Cell Manufacturing. *Semicond. Sci. Technol.* **2012**, *27*, 074002−074002−13.

(19) Bae, D.; Kwon, S.; Oh, J.; Kim, W.; Park, H. Investigation of Al_2O_3 Diffusion Barrier Layer Fabricated by Atomic Layer Deposition for Flexible Cu(In,Ga)Se$_2$ Solar Cells. *Renewable Energy* **2013**, *55*, 62−68.

(20) Thimsen, E.; Baryshev, S.; Martinson, A.; Elam, J.; Veryovkin, I.; Pellin, M. Interfaces and Composition Profiles in Metal-Sulfide Nanolayers Synthesized by Atomic Layer Deposition. *Chem. Mater.* **2013**, *25*, 313−319.

(21) Thimsen, E.; Riha, S.; Baryshev, S.; Martinson, A.; Elam, J.; Pellin, M. Atomic Layer Deposition of the Quaternary Chalcogenide Cu_2ZnSnS_4. *Chem. Mater.* **2012**, *24*, 3188−3196.

(22) Yousfi, E. B.; Weinberger, B.; Donsanti, F.; Cowache, P.; Lincot, D. Atomic Layer Deposition of Zinc Oxide and Indium Sulfide Layers for Cu(In,Ga)Se$_2$ Thin-Film Solar Cells. *Thin Solid Films* **2001**, *387*, 29−32.

(23) Asikainen, T.; Ritala, M.; Leskela, M. Growth of In_2O_3 Thin-Films by Atomic Layer Epitaxy. *J. Electrochem. Soc.* **1994**, *141*, 3210−3213.

(24) Aarik, J.; Aidla, A.; Kukli, K.; Uustare, T. Deposition and Etching of Tantalum Oxide-Films in Atomic Layer Epitaxy Process. *J. Cryst. Growth* **1994**, *144*, 116−119.

(25) Aarik, J.; Kukli, K.; Aidla, A.; Pung, L. Mechanisms of Suboxide Growth and Etching in Atomic Layer Deposition of Tantalum Oxide from $TaCl_5$ and H_2O. *Appl. Surf. Sci.* **1996**, *103*, 331−341.

(26) Abou-Ras, D.; Rudmann, D.; Kostorz, G.; Spiering, S.; Powalla, M.; Tiwari, A. N. Microstructural and Chemical Studies of Interfaces between Cu(In,Ga)Se$_2$ and In_2S_3 Layers. *J. Appl. Phys.* **2005**, *97*, 084908−084908−8.

(27) Spiering, S.; Hariskos, D.; Powalla, M.; Naghavi, N.; Lincot, D. Cd-Free Cu(In,Ga)Se$_2$ Thin-Film Solar Modules with In_2S_3 Buffer Layer by ALCVD. *Thin Solid Films* **2003**, *431*, 359−363.

(28) Barreau, N.; Bernede, J.; Marsillac, S.; Mokrani, A. Study of Low Temperature Elaborated Tailored Optical Band Gap β-$In_2S_{3-3x}O_{3x}$ thin films. *J. Cryst. Growth* **2002**, *235*, 439−449.

(29) Mahfouz, R.; Al-Ahmari, S.; Al-Fawaz, A.; Al-Othman, Z.; Warad, I.; Siddiqui, M. Kinetic Analysis for Non-Isothermal

Decomposition of Unirradiated and Gamma-Irradiated Indium Acetyl Acetonate. *Mater. Res.* **2011**, *14*, 7−10.

(30) Dasgupta, N.; Mack, J.; Langston, M.; Bousetta, A.; Prinz, F. Design of an Atomic Layer Deposition Reactor for Hydrogen Sulfide Compatibility. *Rev. Sci. Instrum.* **2010**, *81*, 044102.

(31) Barry, S. T.; Gordon, P. G.; Ward, M. J.; Heikkila, M. J.; Monillas, W. H.; Yap, G. P. A.; Ritala, M.; Leskela, M. Chemical Vapour Deposition of In_2O_3 Thin Films from a Tris-Guanidinate Indium Precursor. *Dalton Trans.* **2011**, *40*, 9425−9430.

(32) Riha, S. C.; Libera, J. A.; Elam, J. W.; Martinson, A. B. F. Design and Implementation of an Integral Wall-Mounted Quartz Crystal Microbalance for Atomic Layer Deposition. *Revi. Sci. Instrum.* **2012**, *83*, 094101−094101−8.

(33) Nelson, A. Co-Refinement of Multiple-Contrast Neutron/X-ray Reflectivity Data Using MOTOFIT. *J. Appl. Crystallogr.* **2006**, *39*, 273−276.

(34) Ott, A.; Johnson, J.; Klaus, J.; George, S. Surface Chemistry of In_2O_3 Deposition Using $In(CH_3)_3$ and H_2O in a Binary Reaction Sequence. *Appl. Surf. Sci.* **1997**, *112*, 205−215.

(35) Lee, D.; Kwon, J.; Lee, J.; Kim, K. Self-Limiting Film Growth of Transparent Conducting In_2O_3 by Atomic Layer Deposition using Trimethylindium and Water Vapor. *J. Phys. Chem. C* **2011**, *115*, 15384−15389.

(36) Chi, W. H.; Yen, K. Y.; Su, H. L.; Li, S. C.; Gong, J. R. On the Physical Properties of In_2O_3 Films Grown on (0001) Sapphire Substrates by Atomic Layer Deposition. *J. Vac. Sci. Technol. A* **2011**, *29*, 03A105.

(37) Elam, J. W.; Martinson, A. B. F.; Pellin, M. J.; Hupp, J. T. Atomic Layer Deposition of In_2O_3 using Cyclopentadienyl Indium: A New Synthetic Route to Transparent Conducting Oxide Films. *Chem. Mater.* **2006**, *18*, 3571−3578.

(38) Libera, J. A.; Hryn, J. N.; Elam, J. W. Indium Oxide Atomic Layer Deposition Facilitated by the Synergy between Oxygen and Water. *Chem. Mater.* **2011**, *23*, 2150−2158.

(39) Lim, B.; Rahtu, A.; Gordon, R. Atomic Layer Deposition of Transition Metals. *Nat. Mater.* **2003**, *2*, 749−754.

(40) Lim, B.; Rahtu, A.; Park, J.; Gordon, R. Synthesis and Characterization of Volatile, Thermally Stable, Reactive Transition Metal Amidinates. *Inorg. Chem.* **2003**, *42*, 7951−7958.

(41) Kissounko, D.; Zabalov, M.; Brusova, G.; Lemenovskii, D. Principal Trends in Chemistry of Amidinate Complexes of Main-Group and Transition Elements. *Usp. Khim.* **2006**, *75*, 395−421.

(42) Zhou, Y.; Richeson, D. S. Bulky Amidinate Complexes of Indium(III). Synthesis and Structure of $[CyNC(^tBu)NCy]_2InCl$. *Inorg. Chem.* **1996**, *35*, 2448−2451.

(43) Meng, X.; Libera, J. A.; Fister, T. T.; Zhou, H.; Hedlund, J. K.; Fenter, P.; Elam, J. W. Atomic Layer Deposition of Gallium Sulfide Films Using Hexakis(dimethylamido)digallium and Hydrogen Sulfide. *Chem. Mater.* **2014**, *26*, 1029−1039.

(44) Stuyven, G.; De Visschere, P.; Hikavyy, A.; Neyts, K. Atomic Layer Deposition of ZnS Thin Films Based on Diethyl Zinc and Hydrogen Sulfide. *J. Cryst. Growth* **2002**, *234*, 690−698.

(45) Kim, J.; George, S.; Greene, L.; Sherif, R. Tin Monosulfide Thin Films Grown by Atomic Layer Deposition Using Tin 2,4-Pentanedionate and Hydrogen Sulfide. *J. Phys. Chem. C* **2010**, *114*, 17597−17603.

(46) The International Center for Diffraction Data. Powder Diffraction File (PDF) 00-025-0390.

(47) Okamoto, H. In-S (Indium-Sulfur). *J. Phase Equilib. Diffus.* **2013**, *34*, 149−150.

(48) Patterson, A. L. Scherrer Formula for X-ray Particle Size Determination. *Phys. Rev.* **1939**, *56*, 978−982.

(49) Zhao, Z.; Cao, Y.; Yi, J.; He, X.; Ma, C.; Qiu, J. Band-Edge Electronic Structure of β-In_2S_3: The Role of s or p Orbitals of Atoms at Different Lattice Positions. *ChemPhysChem* **2012**, *13*, 1551−1556.

(50) Lee, J.; Lee, J.; Ahn, B.; Kim, K. Structural and Optical Properties of β-In_2S_3 and β-In_2S_3:CO^{2+} Films Prepared on Indium-Tin-Oxide Substrates. *J. Korean Phys. Soc.* **2008**, *53*, 3255−3261.

(51) Bedir, M.; Oztas, M. Effect of Air Annealing on the Optical Electrical and Structural Properties of In_2S_3 Films. *Sci. China, Ser. E* **2008**, *51*, 487−493.

(52) Rehwald, W.; Harbeke, G. On the Conduction Mechanism in Single Crystal β-Indium Sulfide In_2S_3. *J. Phys. Chem. Solids* **1965**, *26*, 1309−1324.

(53) Jayakrishnan, R.; John, T.; Kartha, C.; Vijayakumar, P.; Abe, T.; Kashiwaba, Y. Defect Analysis of Sprayed Beta-In_2S_3 Thin Films Using Photoluminescence Studies. *Semicond. Sci. Technol.* **2005**, *20*, 1162−1167.